Science & Technology Facilities Council

Technical Report
RAL-TR-2016-003

Simulations of Muon production targets

A Bungau, R Cywinski, C Bungau, JS Lord, SP Cottrell, AD Hillier, JNT Peck,

April 2016

Enquiries concerning this report should be addressed to:

RAL Library
STFC Rutherford Appleton Laboratory
Harwell Oxford
Didcot
OX11 0QX

Tel: +44(0)1235 445384
Fax: +44(0)1235 446403
email: libraryral@stfc.ac.uk

Science and Technology Facilities Council reports are available online at: http://epubs.stfc.ac.uk

ISSN 1358-6254

Simulations of Muon production targets

Adriana Bungau, Robert Cywinski, and Cristian Bungau
University of Huddersfield, School of Applied Sciences, Huddersfield, HD1 3DH, United Kingdom

James S. Lord, Stephen P. Cottrell, Adrian D. Hillier, and Jamie N. T. Peck
ISIS Neutron and Muon Source, STFC-Rutherford Appleton Laboratory, Didcot, OX11 0QX, United Kingdom
(Dated: March 29, 2016)

We review the recent simulations of muon production targets using the GEANT4 framework. Options for modifying the ISIS target are considered, as well as a wider study considering different materials, geometries and incident beam energies.

I. INTRODUCTION

Intense beams of polarised muons are required by the muon spin rotation, relaxation or resonance (μSR) technique to probe materials in the bulk in order to tackle fundamental problems in condensed matter science, chemistry, medicine and particle physics [1–7]. The μSR technique uses the muon's spin to examine the structural and dynamical processes in bulk materials on the atomic and subatomic scale. Muons are implanted into a sample material and their spins precess around the local atomic and nuclear magnetic fields. The unstable muons decay with an average lifetime of 2.2 μs into a positron. Since these positrons are emitted preferentially in the direction of the muons' spin, the precessional motion can be followed simply by observing their angular and time dependent distribution. μSR, at the existing muon facilities, has made major contributions to our understanding of a diverse range of phenomena such as superconductivity, itinerant magnetism, semiconductors etc. [8–15] If, however, more intense muon beams were routinely available it would enable rapid parametric investigations as a function of magnetic field or temperature, for example [16], and be beneficial for novel muon methods, such as low energy beams or experiments that exploit pulsed stimuli.

μSR experiments generally (though not always) rely upon polarised beams of relatively low energy positive muons which rapidly thermalise within 1 mm after entering the sample being studied. An intense source of such polarised muons, known as surface muons with momenta of $\approx$28 MeV/c, is produced by the decay of positive pions which are at rest at the surface of the production target. The polarised surface muons, initially exiting in all directions, are focused and guided with magnetic fields to the muon spectrometers.

For muon experiments involving high pressure cells and similar complex sample environment equipments, penetrating high momentum muon beams are required. In this case decay muon beams are used, where the pions from the target are collected into a beam and allowed to decay in flight. Selection of the momentum of both the pions and the resulting muons allows selection of those produced by forward (or backward) decays which have a high polarisation.

μSR experiments can be carried out at the continuous muon beam facilities at PSI (Switzerland) [17] and TRIUMF (Canada) [18], or at the pulsed beam facilities at ISIS (UK) [19] and J-PARC (Japan) [20]. The high cost related to accelerator construction and operation have resulted in the so-called multipurpose facilities where muon experiments are carried out alongside others such as neutron scattering, providing complementary information in a wide variety of scientific applications. As a result of this coexistence, the design of each of the muon facilities, such as the geometry and efficiency of the pion/muon target and the energy and time structure of the proton beam, is essentially a compromise which leads to a sub-optimal muon delivery rate to the μSR spectrometers [21].

Therefore it is of technical interest to consider how muon production can be optimised. Using the ISIS target as a reference, simulations have been performed to provide an optimised solution for the target design with respect to pion/muon production. Implications of the optimised solutions for the ISIS facility are also discussed in this paper.

The development of these simulations will be essential if the full potential of the next generation sources is to be realised. Using the methods discussed here, the potential for muon production at the ESS might be investigated in future work, and compared to the utility of a stand alone facility (perhaps co-located with other large facilities to benefit from scirntific and technical support), optimised specifically for muon production for μSR experiments.

II. SIMULATION CODES

Optimisation studies were performed using the Monte Carlo code GEANT4 [22], which simulates particle interactions and transport through the target material. Pion production differential cross sections for 730 MeV proton energy were modelled using three physics packages: QGSP-BERT [23] , QGSP-BIC‘[24], and QGSP-INCL-ABLA [25].

The results were validated against experimental data from Cochran et al. [26], who performed experiments at the Lawrence Radiation Laboratory cyclotron which measured the pion production cross-sections on targets

over a wide range of production angles and pion energies. The experiment used a proton beam extracted from a cyclotron, a selected target material and a pion spectrometer consisting of a bending magnet and an array of 12 counter telescopes. The eleven target materials used were liquid H_2, CD_2, Be, C, Al, Ti, Cu, Ag, Ta, Pb and Th. The spectrometer was repositioned to select pions emitted at one of several angles with respect to the proton beam. The measured differential cross-sections for pion production by 730 MeV protons on targets provided a reliable guide for the design of pion beams at various meson facilities.

Validation results are shown in Fig. 1 and demonstrate good agreement between simulation and experimental data for version geant4.9.3.p02 [27]; however, for later releases (versions geant4.9.4.p04, geant4.9.5.p02 and geant4.9.6.p01) the results are noticeably different. In these releases the function *getMomModuleFor2toMany* from the class *G4ElementaryParticleCollider* has been modified by eliminating a special case initialisation to obtain better agreement with data for pion and kaon interactions with hadrons at the higher end of the kinematic range. However, this modification significantly changed the comparison of Bertini model output to data for hadron-nucleon cascades [28].

At small angles the previous versions geant4.9.3.p02 and geant4.9.4.p04 seem to be in reasonably good agreement with the experimental data for all three cascade models. Versions geant4.9.5.p02 and geant4.9.6.p01 however show significant discrepancies especially for Bertini and Binary Cascade models. At large angles the QGSP-BERT package gives a better agreement with data while QGSP-BIC tends to overestimate pion production. The QGSP-INCL-ABLA package also overestimates the data, apart from version geant4.9.6.p01 where the experimental results are underestimated. Therefore, in our simulations we used the version geant4.9.3.p02 with the QGSP-BERT package, as this is demonstrably more reliable for our particular problem. This package comprises several physics models:

- the Bertini Cascade Model (BERT) for intranuclear cascade followed by pre-equilibrium and evaporation phases of the residual nucleus for proton, neutron, pion and kaon interactions below 9.9 GeV;
- parameterised models for all remaining hadrons;
- parameterised capture and fission for low energy neutrons;
- hadronic elastic scattering;
- standard electromagnetic physics;
- Chiral Invariant Phase Space (CHIPS) model of nuclear capture of negatively charged particles at rest;
- parameterised muon-nuclear interactions;
- CHIPS model for gamma-nuclear and electron-nuclear interactions;
- Quark-Gluon String (QGS) model for all hadronic interactions above 12 GeV followed by the Precompound model for pre-equilibrium and evaporation phases of the residual nucleus;
- Low Energy Parameterised model for hadronic interactions between 9.5-25 GeV;
- quasi-elastic scattering.

III. OPTIMISING PROTON ENERGY

A. Proton Transmission

Muon production targets are typically used in transmission, with the transmitted proton beam being used for production of other particles. For example, at ISIS, only 4% of the proton beam is used for muon production, with the remaining protons producing spallation neutrons. Therefore, for a muon target at a shared facility it is desirable to optimise the number of muons produced while keeping in mind the limitations of the target geometry and proton transmission. An optimisation of the collection geometry might also be advantageous.

Simulations were carried out to investigate proton beam transmission as a function of proton energy and target thickness [27]. For convenience, the ISIS target geometry (discussed in section VI) was modelled, using graphite as the target material oriented at 45° to the proton beam. An incident proton beam having 10^9 protons at the required energy and with zero energy spread (the actual value at ISIS is 1 MeV) was used, with protons considered to be transmitted if scattered through an angle less than 28.8 mrad allowing them to pass through downstream collimation (discussed further in section VI).

Simulation results shown in Fig. 2(a) confirm that proton transmission through a graphite target increases with proton energy. The result suggests that thicker targets could be used at higher energies. Further simulations were carried out to investigate this, with the target thickness for 96% proton transmission shown as a function of proton energy (Fig. 2(b)). As expected, muon production on future multipurpose high power sources can realise an immediate benefit from the ability to use thicker muon production targets while maintaining proton transmission. However, for the purposes of this study, the target thickness was not generally varied with proton energy. Instead, the variation of pion or muon yield was compared with the proton beam loss.

B. Pion Production

Simulations were carried out to investigate pion yield within the production target as a function of proton beam

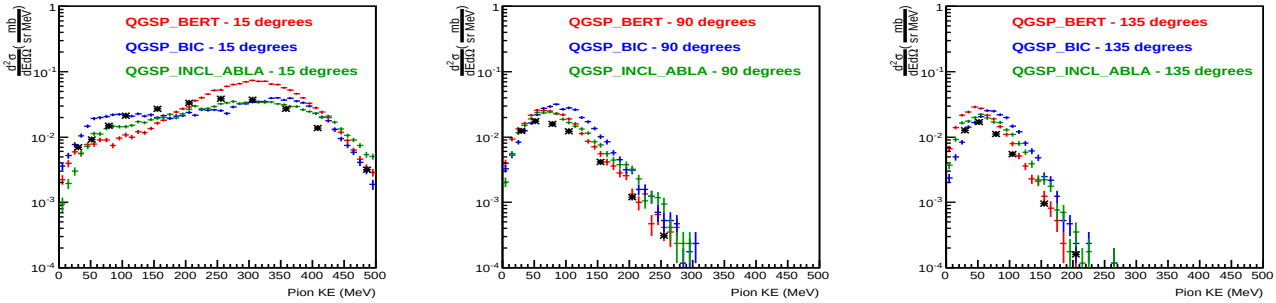

(a)Pion production double differential cross section using the GEANT4 version geant4.9.3.p02.

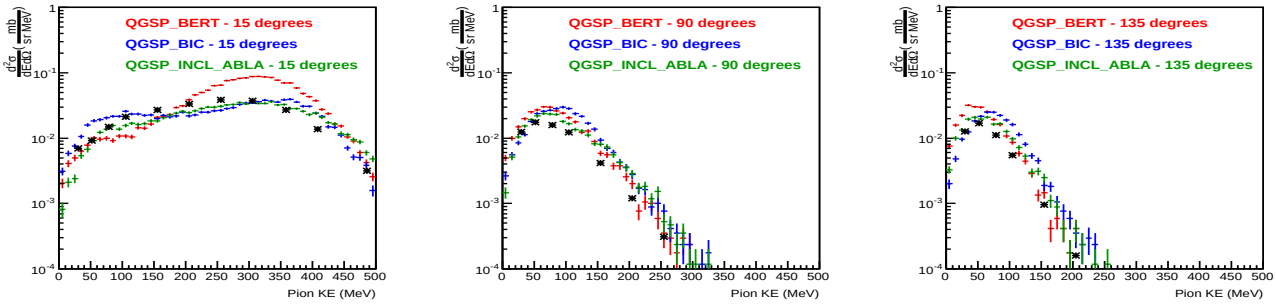

(b)Pion production double differential cross section using the GEANT4 version geant4.9.4.p04.

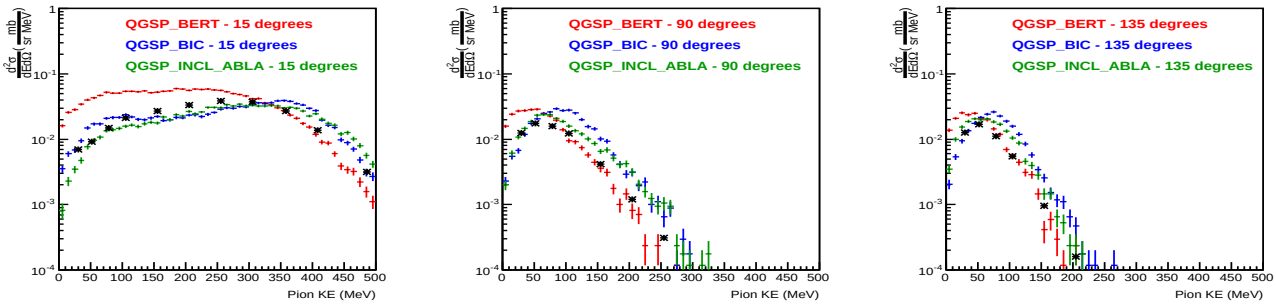

(c)Pion production double differential cross section using the GEANT4 version geant4.9.5.p02.

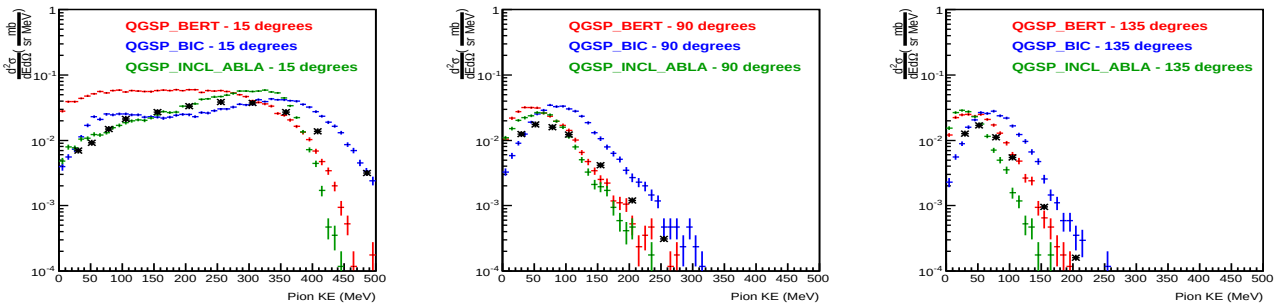

(d)Pion production double differential cross section using the GEANT4 version geant4.9.6.p01.

FIG. 1. Double differential cross-section predictions with the last four GEANT4 versions for positive pion production. Three physics packages (QGSP-BERT, QGSP-BIC, QGSP-INCL-ABLA) are compared with experimental data.

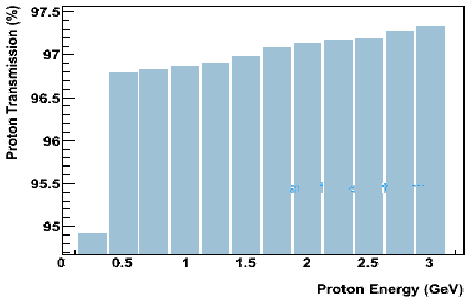

(a)Transmission through a 7 mm graphite target.

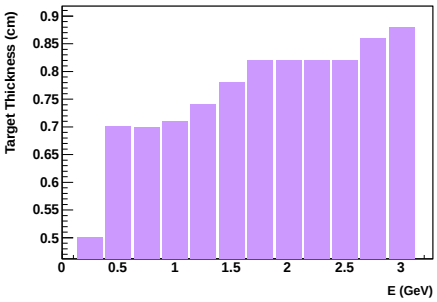

(b)Graphite target thickness for 96% proton transmission.

FIG. 2. Proton transmission as a function of the proton beam energy.

energy. The threshold for single pion production that results from proton-nucleon interactions inside the target is typically 280 MeV (or twice the pion mass) in the laboratory frame. This is clearly seen in the simulation results shown in Fig. 3, which also demonstrate that the pion yield increases rapidly with energy once beyond this threshold.

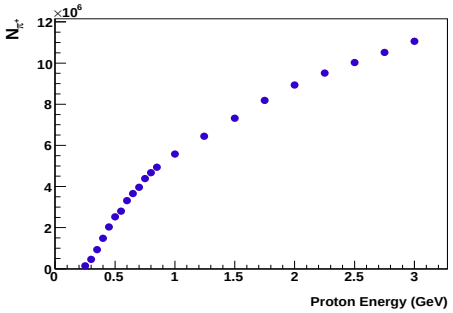

FIG. 3. Variation of pion yield with proton energy.

To obtain the maximum number of single pions, the incident proton beam should have an energy in the range 500-800 MeV. At higher energies it is possible to produce pions in pairs. Double pion production reactions occur only when there is sufficient energy in the collision, and are typical for proton energies beyond 1 GeV. This is demonstrated by the simulations shown in Fig. 4, where the momenta and energy spectra of the pions is shown for various incident proton energies.

The onset of the double pion production at 750 MeV (Fig. 4(a)) is seen by the shoulder in the curve, while the double pion production peak becomes prominent at 1 GeV incident proton energy and above (Fig. 4(b)).

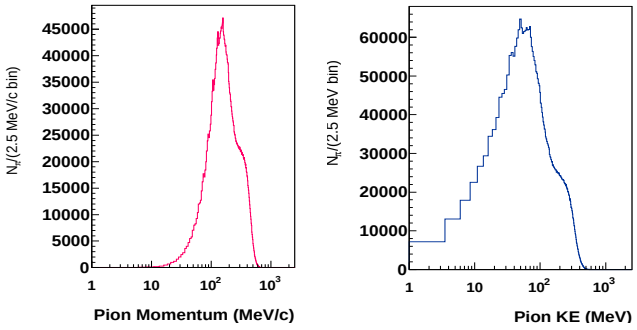

(a)750 MeV

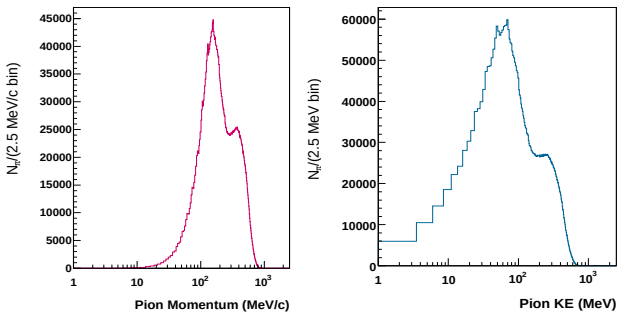

(b)1 GeV

FIG. 4. Pion momentum and energy spectra for various incident proton energies.

The momentum spectrum and angular distribution of the pions produced depend on the primary proton beam energy, and therefore simulations were performed using several incident proton energies. Energies were chosen to correspond to the incident proton beam characteristics of the TRIUMF, ISIS and J-PARC accelerators (Figs. 5(a)–(c) respectively). Pions exiting the target at angles smaller than 20 degrees, or higher than 160 degrees, with respect to the proton beam were recorded (Fig. 5). Pion production is forward biased, and the forward-backward asymmetry increases with the energy of the proton beam. The momentum distribution of the pions exiting the target at angles larger than 160 degrees is a single gaussian. The average momentum increases from 122 MeV/c for 500 MeV protons to 160 MeV/c for 3 GeV protons. For the pions coming out of the target at angles smaller than 20 degrees, the momentum

distribution for 3 GeV protons can be approximated by a superposition of three Gaussians, one centered at 150 MeV/c, one at ∼500 MeV/c and one at ∼1 GeV/c.

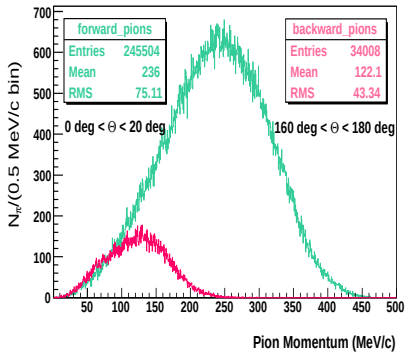

(a). 500 MeV incident protons.

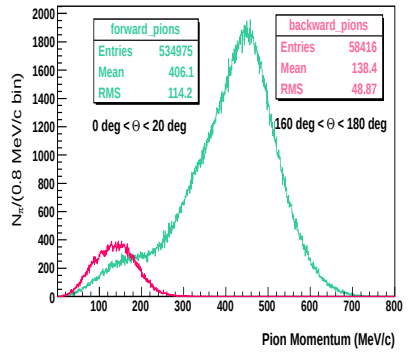

(b). 800 MeV incident protons.

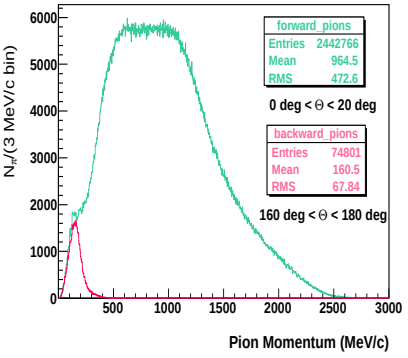

(c). 3 GeV incident protons.

FIG. 5. Pion momentum distributions at various incident proton energies.

C. Muon Production

A fraction of the pions produced inside the target have low energy, stopping within the target after having completely lost their momentum inside the target itself. They decay at rest producing monoenergetic muons with a high polarization in their direction of travel, and those muons formed close to the sample surface may escape. Another fraction of pions decay in flight in the free space close to the production target, and because the momentum of the parent pion is unknown, the muons produced (known as cloud muons) have a lower net polarisation.

The muons produced by pions decaying at rest near the target surface have sufficient energy to escape from inside the target and are known in literature as surface muons. Only positive surface muons can be produced because any negative pions stopped inside the target are rapidly captured by the nuclei. Surface muons have a momentum range 0-30 MeV/c, with the spread resulting from the depth from which the muons escape, and the muon beam has a high intensity due to the high stopping pion density inside the target.

Simulations were carried out to investigate surface muon production as a function of proton energy. To ensure a proper count of muon production, simulations modelled a target surrounded by a spherical detector shell of inner radius 14 cm and outer radius 16 cm. The shell contained a vacuum to avoid particle scattering affecting the result. The total yield for surface muons and muons from pions decaying in flight with a momentum lower than 30 MeV/c is shown in Fig. 6(a). A peak at an incident proton energy of about 500 MeV can be observed.

Increasing the proton energy above this value merely produces more high momentum pions in the forward direction, most of which are well outside the momentum range likely to be used by a decay beam, though there is a small increase in the 50–200 MeV/c range. At higher proton beam energies, most pions have high kinetic energy and escape the target rather than coming to rest and having time to decay to surface muons. A normalisation to the incident proton energy is shown in Fig. 6(b), with a clear peak in the yield at about 500 MeV.

Since the proton transmission is a function of the proton energy, a normalisation to the number of protons interacting in the target was also investigated, and it also shows a peak at about 500 MeV (Fig. 6(c)). This normalisation was performed in order to calculate the average number of muons produced in a proton interaction inside the target as a function of incident proton energy. Therefore, for surface muon production, TRIUMF obtains a higher muon yield at 500 MeV than ISIS at 800 MeV, with only a marginal benefit at 3 GeV (J-PARC). Because the muon yield starts to increase above 1 GeV, the study was extended to higher proton energies to look for a second peak in muon production. However, a continuous increase in muon yield with proton energy was found up to 9 GeV (Fig. 7(a)). The normalisation of the

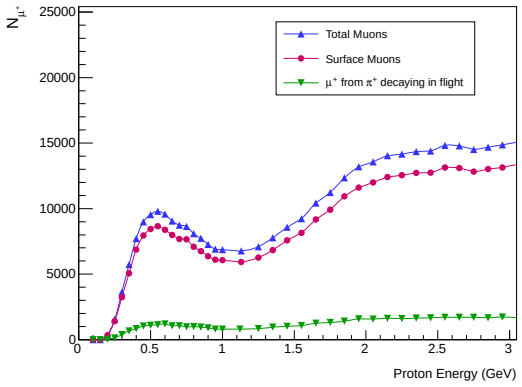

(a). Raw muon yield per 10^9 protons.

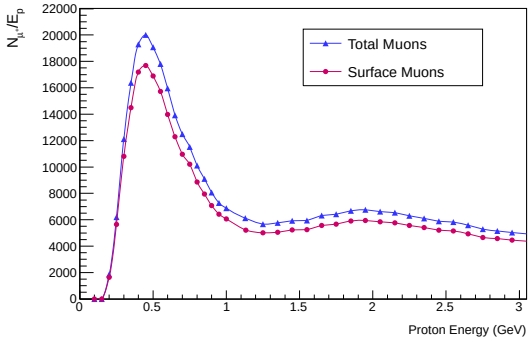

(b). Muon yield normalised to the proton energy.

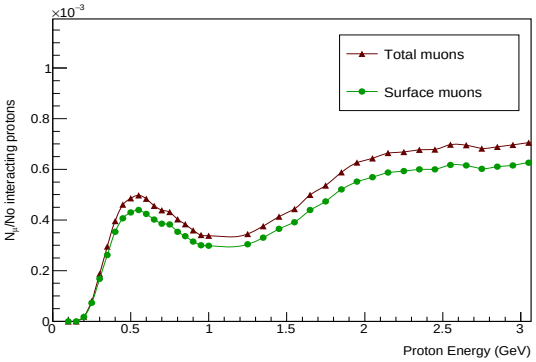

(c). Muon yield normalised to the number of protons interacting in the target.

FIG. 6. Variation of muon yield with proton energy.

muon yield to the incident proton energy shows a single peak at about 500 MeV (Fig. 7(b)) and there is clearly no gain in going to higher energies for this particular target geometry and material.

Momentum distributions of the surface muons produced by the incident proton beam of energies used at TRIUMF, ISIS and J-PARC accelerators are shown in Figs. 8(a)–(c) respectively. Simulations recorded the surface muons emitted in the forward direction at an angle smaller than 20 degrees with respect to the proton beam and in the backward direction at an angle higher than 160 degrees. For pion production, the forward-backward asymmetry increases with the proton energy, while in the case of muons, muon rates and momentum distributions are similar for all three proton energies, while the absolute number of muons produced clearly reflect the results of simulations shown in Fig.6 This suggests that surface muon production is close to isotropic, which might be expected from a pion (spin 0) at rest.

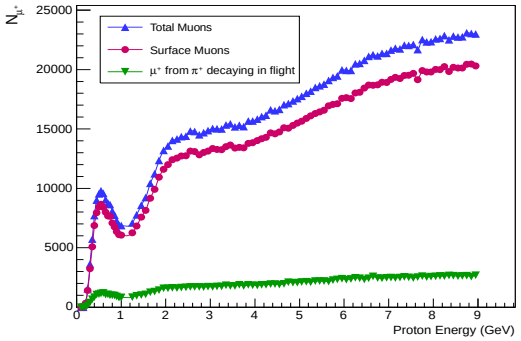

(a). Raw muon yield.

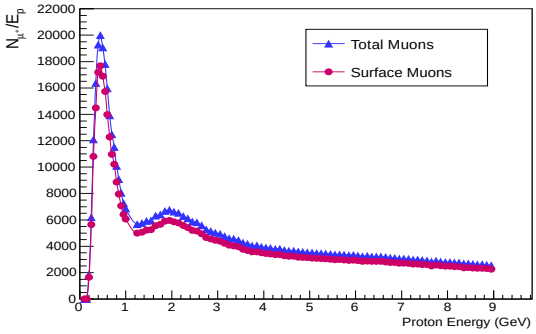

(b). Yield normalised to proton energy.

FIG. 7. Variation of muon yield with proton energy at higher energies.

IV. MATERIAL CHOICE

A substantial gain in intensity can be achieved through optimisation of the target material. At current muon facilities, low-Z materials like graphite and beryllium were chosen for the target as both have a low density, allowing the proton beam to pass through the target without significant interaction. Additionally, both materials have a high melting point, 3800 K for graphite and 1560 K for beryllium, essential as the target is expected to run hot in vacuum. Beryllium, in particular, also has a high temperature stability and a low coefficient of expansion with temperature. For a stand alone muon target, nickel might also be considered as a potential candidate due to the high melting point (1726 K) and stress resistance.

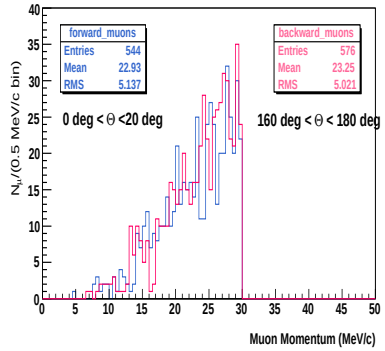

(a). 500 MeV incident protons (TRIUMF).

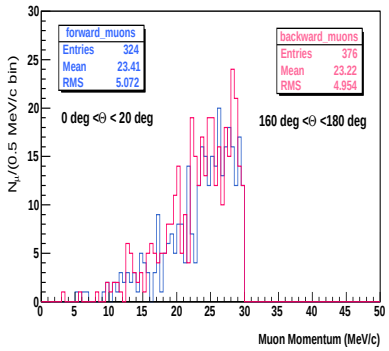

(b). 800 MeV incident protons (ISIS).

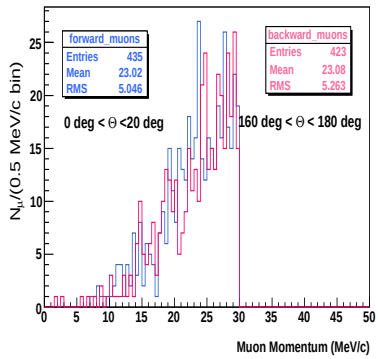

(c). 3 GeV incident protons (J-PARC).

FIG. 8. Surface muon momentum distributions for incident proton energies reflecting the proton beam at existing facilities

Low-Z target materials are preferred for production targets as they maximise pion production while minimising both the rate of absorption of secondary pions and multiple scattering of the proton beam itself within the muon target. The material properties must also be suitable for operating in the extreme conditions of an intense high energy pulsed proton beam — providing efficient energy dissipation and surviving both the pressure waves induced by beam pulses and the long-term effects of radiation damage.

Simulations were carried out to investigate muon yield as a function of target thickness, with the production efficiency of various materials being investigated [29]. Simulations were set up in a similar manner — a Gaussian beam was formed of 10^9 protons with a radius of 10 mm, and the target was surrounded by vacuum including a spherical detector with inner radius 13 cm and outer radius 14 cm.

The variation of the total and surface muon yield as a function of target thickness is shown in Fig. 9(a). All muons having momentum in the range 0-100 MeV/c are recorded in the shell. Selecting only those muons with momentum below 30 MeV/c enables a count of both the surface muons produced by pions decaying at rest near the target surface with sufficient energy to escape from inside the target, together with background "cloud" muons (muons coming from pions in flight and having a momentum lower than 30 MeV/c). Results suggest that a nickel target would give a substantially higher muon yield compared to those obtained from graphite and beryllium. For example, a 30 mm Ni target would produce four times more surface muons than a 7 mm graphite target. However, as a high-Z material, proton transmission would be compromised thus making it more suited to a stand alone muon facility.

Target thickness can also be expressed in terms of the number of proton interaction lengths and the corresponding muon yields can be compared for the same number of interaction lengths in the three materials. The muon yield, given by the same number of proton inelastic interactions in these materials, enables us to compare the muons produced per interaction, rather than target thickness, giving a measure of efficiency for muon production. From Fig. 9(b) it can be seen that the muon yield per proton interaction is lower in beryllium than in both graphite and nickel. It is clear that a comprehensive study of different target configurations which addresses all the engineering aspects of each solution should be carried out as a continuation of this work.

V. TARGET GEOMETRY AND ANGLE

Since surface muon production at small target thicknesses is nonlinear, the muon yield might be improved by splitting the target into two or three slabs such that the total thickness remains equivalent to the single slab. By doing so, more pions decaying at rest will be close to a surface, thus enhancing surface muon production without compromising beam transmission. Simulations were carried out using a similar geometry to that described in section IV and modelling proton beam interaction with graphite slabs of total thickness 7 mm presented at 45° to the proton beam. Muon yield was investigated as a function of the number of slabs and their separation, with

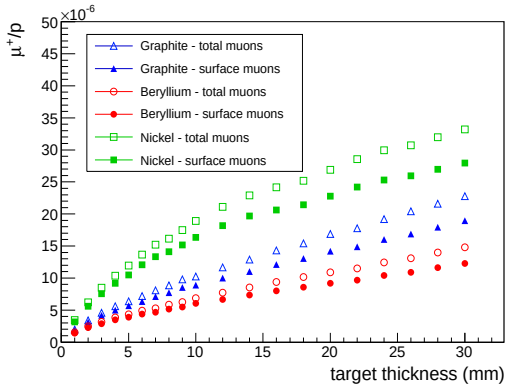

(a). Variation of the muon yield with the target thickness.

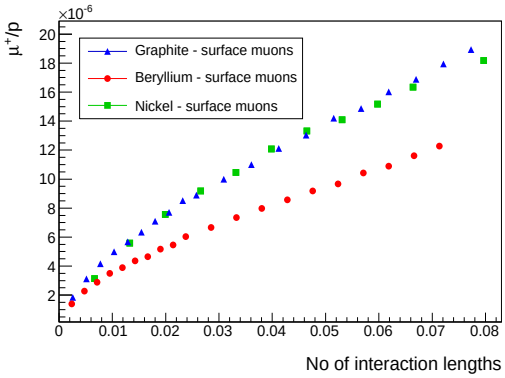

(b). The muon yield as a function of the interaction length.

FIG. 9. The comparison of the muon yield per proton for three different materials.

results shown in Fig. 10.

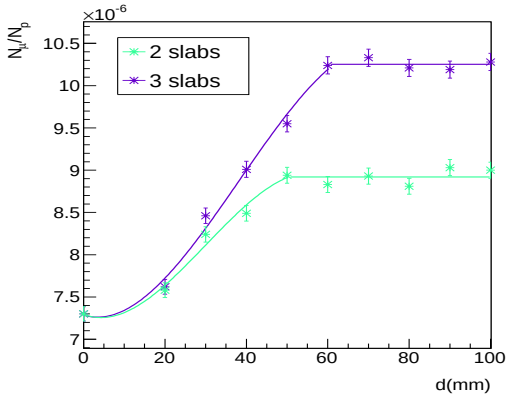

FIG. 10. Variation of the surface muon yield with the slab separation distance. The muons are detected by the spherical shell.

For small slab separations, a fraction of the surface muons are implanted into an adjacent slab and so do not reach the shell. Therefore, the surface muon yields for two and three slabs are similar when the separation distance is below 20 mm. As the distance is increased the muon detection rate rises and then flattens as all the muons produced in the slabs reach the detector. Compared to the standard geometry, surface muon production can theoretically be increased by 21% and 40% by segmenting into two and three slabs respectively.

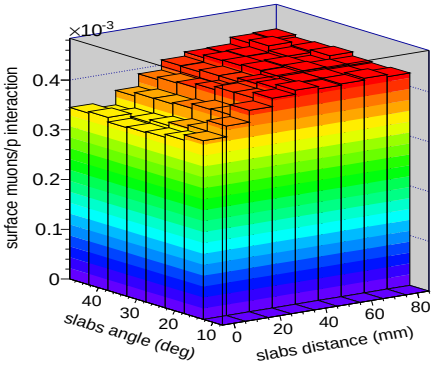

(a). The two slab design.

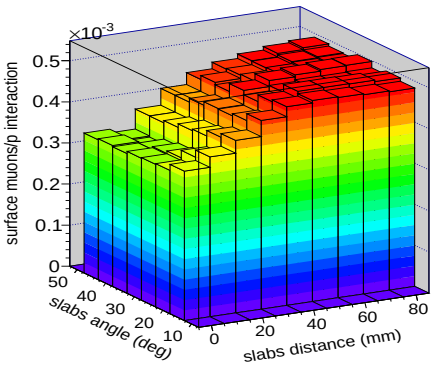

(b). The three slab design.

FIG. 11. Variation of the surface muon yield with distance between the slabs and slabs angle orientation for a 2-slab design (a) and a 3-slab design (b).

The simulations up to now involved a target of 7 mm thickness. By adjusting the target orientation, different slab thicknesses can be presented in the beam path, thus leading to more proton interactions inside the target and a higher surface muon yield. Results of further simulations designed to study surface muon yield as a function of slab separation and orientation are shown in Fig. 11. For the smallest angles, a higher total slab thickness is presented in the proton beam path leading to an increase in flux (and a corresponding increase in proton beam loss).

While these simulations show clear advantages in using a target comprising more than one slab, for a practical muon beamline muons must be collected and focused

onto a sample. Being able to collimate to suit small sample sizes without significant loss of intensity is an advantage. This becomes difficult for a target assembly with multiple distinct regions where muons are produced, and is therefore not obviously the best choice for a practical beamline.

VI. OPTIMISATION FOR ISIS AND FUTURE FACILITIES

The optimised solutions described previously have been implemented in simulations of the ISIS muon target. The pulsed muon facility at ISIS facility has operated successfully for many years serving an international μSR community. During operation, the ion source of the ISIS accelerator injects negatively charged hydrogen ions into a linac which accelerates and transports the ions to the synchrotron where, on injection, they are stripped of their electrons by a thin foil, leaving bare protons. The synchrotron then accelerates the protons to 800 MeV. The resulting extracted proton beam has a double pulse structure with 2.5×10^{13} protons per double pulse, with a frequency of 50 Hz, resulting in a nominal proton beam current of 200 μA. (One pulse in 5 is sent to a second target station, resulting in the muon target receiving 160 μA proton beam current at a mean repetition rate of 40 Hz.)

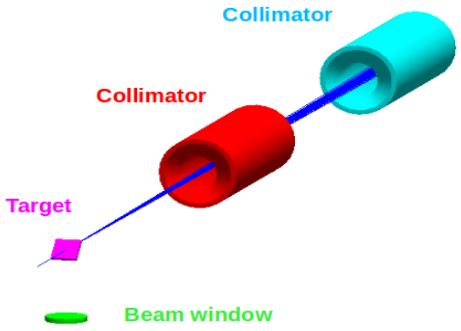

FIG. 12. GEANT4 modelling of the ISIS muon target, beam window and collimators. The target is tilted at 45 degrees and the muons produced in the target are collected by the beam window. The transmitted proton beam passes through the collimation system and impacts further on the neutron target situated 20 m downstream.

The extracted proton beam then passes through a thin graphite muon production target with dimensions 50×50×7 mm, oriented at 45 degrees to the proton beam and giving an effective length of 10 mm along the beam (Fig. 12). The interaction of the proton beam with the target nuclei produces pions which decay into muons. The primary requirement for the target is to produce a large number of pions and hence muons in order to achieve acceptable intensities for experiments.

The surface muons produced at the target are extracted into two beam lines each at 90 degrees with respect to the proton beam. One port serves the EU facility [30], comprising three instruments that are fully scheduled for condensed matter experiments, the second port provides beam for the RIKEN-RAL facility [31], with four end stations carrying out various condensed matter and nuclear physics research. The muon beam is fully polarised and the polarisation is maintained during beam transport. Both beam lines are separated from the main proton beam and target vacuum vessel by a thin aluminium window (typically 60 μm). The beam window has a diameter of 8 cm and is situated 15 cm from one side of the target. The production target is followed by a set of two collimators [27]. The collimators stop any muons and neutrons formed at low angles, or any protons scattered through larger than average angles, which would otherwise hit the beam pipe or quadrupole magnets between the muon and neutron targets. The collimators are angled cones of 40 cm length and are made of Cu. The first collimator has an inner radius of 37.5mm and an outer radius of 54.15 mm and the second collimator has an inner radius of 51 mm and an outer radius of 61.4 mm and intercepts protons at angles greater than 28.8 mrad. Protons exiting the second collimator are considered as transmitted.

The transmitted proton beam goes on to impact the tungsten neutron production target situated 20 m downstream. Because the muon facility is essentially parasitic with respect to the neutron facility, the proton transmission through the muon production target (defined as the fraction of protons passing through the collimation system) must be maintained at a predetermined level to prevent loss in neutron intensity.

The requirement for 96% proton transmission is satisfied by either a 7 mm graphite or beryllium target or a 1.6 mm nickel target. Results shown in Fig. 9, however, demonstrate that a 7 mm graphite target gives a higher surface muon yield than 7mm targets formed from either nickel (1.6 mm) or beryllium (7 mm). However, we have investigated an optimisation of a beryllium target, where a nickel coating is used to prevent evaporation or sputtering of beryllium from the target surface that might contaminate the beamline and create a health hazard. Nickel has been shown to be a suitable coating material for conventional low Z targets. Clearly the nickel coating should be sufficiently uniform and robust to prevent any sputtering and evaporation of beryllium, but at the same time be sufficiently thin so as to not compromise the proton transmission through the composite target. From simulations using a geometry discussed in section III A, we found that a beryllium target of 6 mm thickness encapsulated with 0.5 mm nickel on all surfaces gives a proton transmission of 95.01% for an 800 MeV beam energy. Simulation results for the total and surface muon yield (using the geometry discussed in section III C)for graphite, beryllium, nickel and composite targets for a

comparable proton transmission are presented in Table I.

TABLE I. Total and surface muon yield detected over a spherical shell for a similar proton transmission.

Material	Thickness	$(\mu/p) \times 10^{-6}$	(Surface $\mu/p) \times 10^{-6}$
Graphite	7 mm	8.07±0.09	7.09±0.08
Be	7 mm	5.29±0.07	4.65±0.06
Ni	1.6 mm	5.22±0.07	4.71±0.07
Be, Ni coating	(6+1) mm	6.62±0.08	5.84±0.08

The distribution of surface muon production from the composite target is shown in Fig. 13. The different colours represent the contribution of the two materials to the pion production, irrespective of the material in which the pion decays. The relative contributions of beryllium and nickel to the surface muon yields are 59% and 41% respectively.

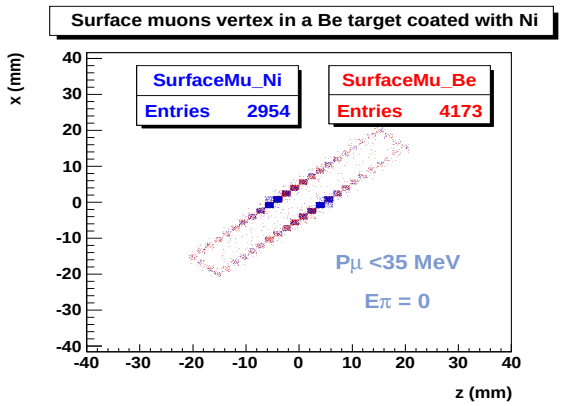

FIG. 13. Contribution of both materials to the surface muon production. Different colours represent the material in which the parent pion was produced.

Simulations were repeated to study muons passing through the ISIS beam window. The simulation geometry was modified with a detector substituting the beam window. The performance of the plain and encapsulated targets is shown in Table II.

TABLE II. Total and surface muon yield at the ISIS beam window for similar proton transmissions.

Material	Thickness	$(\mu/p) \times 10^{-6}$	(Surface $\mu/p) \times 10^{-6}$
Graphite	7 mm	0.18±0.01	0.16±0.01
Be	7 mm	0.13±0.01	0.11±0.01
Ni	1.6 mm	0.11±0.01	0.10±0.01
Be, Ni coating	(6+ 1) mm	0.15±0.01	0.13±0.01

It can be seen that the 7 mm graphite target gives the best performance of all four targets investigated. Results indicate that the ISIS beam window is capturing ∼2% of the total number of surface muons produced in the target. This is as expected since the solid angle to the beam window is $\Omega = 0.071\pi$ and the surface muon production is isotropic [27].

The acceptance of the beam line downstream of the window means that only those muons appearing to come from a region of the target with height ±5 mm and width ±30 mm, as well as with a divergence of 35 mrad in the horizontal direction and 180 mrad in the vertical direction, and momentum in the range 25-27 MeV/c per unit charge, are transmitted to the sample. Selecting only detected muons in this range, for the 7 mm graphite target used at ISIS, approximately 7×10^{-9} surface muons per proton will be delivered to the sample.

Given that graphite appears to be the most efficient target material, we have therefore explored the effect of replacing the current ISIS muon production target with one using two or three graphite slabs. Again we selected only those muons within the source position, angle and momentum ranges appropriate to the real beamline. The results are shown in Fig. 14. Simulations have been carried out for both two and three slabs; in the former case the midpoint between the two slabs was centred on the beamline window axis, while in the latter configuration the centre slab was centred on the window.

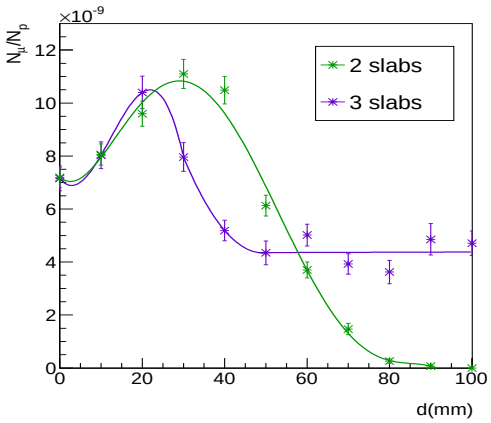

FIG. 14. Variation of the surface muon yield as a function of slab separation for a 45° orientation. Only muons entering the ISIS beam window are detected, and the appropriate selection cuts are applied.

For a two slab geometry, the muon production rate is optimised with a slab distance of ∼30 mm. At greater distances the muons are no longer captured by the 30 mm horizontal acceptance of the beamline and the rate can be seen to fall away. At the optimum distance the surface muon yield could be increased by 54 % compared to the present target design configuration. A three slab target geometry has an optimum muon production rate associated with a 20 mm slab separation, which compared to the current design configuration would give a 50 % increase in surface muon yield. When the distance between the slabs was increased to more than 50 mm, only surface muons emitted by the central slab were collected by the beamline.

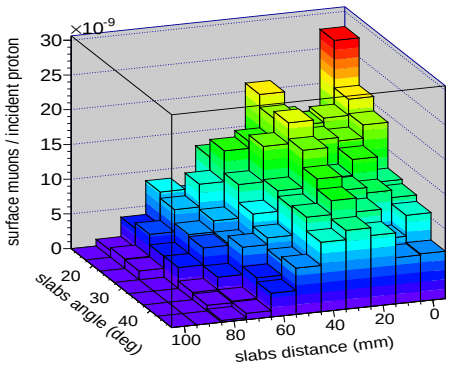

(a). Variation of surface muon yield with slab separation and angle for the two slab design.

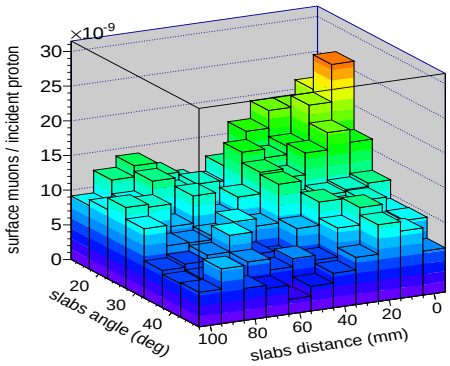

(b). Variation of surface muon yield with slab separation and angle for the three slab design.

FIG. 15. Variation of the surface muon yield accepted by the ISIS beamline as a function of distance between the slabs and slab angle orientation. Results shown for a 2-slabs design (a) and a 3-slabs design (b). Acceptance and angular cuts are applied in both cases.

Since the total thickness of the slabs is always equal to the thickness of the original target (7 mm in the present simulations), the proton transmission does not depend on the number of slabs or on the distance between them, it only depends on their angle of orientation to the proton beam. Targets segmented into two and three slabs, each with a 45 degree angle of orientation with respect to the beam, give a proton transmission of 96.89% and 97% respectively.

The variation of surface muons with the slab separation distance and the angular orientation after applying the acceptance and angular cuts for the ISIS beam window are shown in Fig. 15. Considering that the orientation angle must be larger than 35 degrees in order to maintain the proton transmission above 96%, one can see that an increased muon yield can be obtained for a two-slab design at 35 degrees and 30 mm ($15.5\times10^{-9}\mu/p$) and a three-slab design at 40 degrees and 20 mm ($12.2\times10^{-9}\mu/p$). The surface muon yield doubles for the two slab design case. It should be noted, however, that our simulations are based upon the existing ISIS muon beam line optics. Substantially higher muon beam intensities might be achieved if the beam optics were optimised specifically for the multiple slab geometries.

VII. CONCLUSION

We have modelled muon production by protons on a solid target using the GEANT4 package. We find a peak in muon production for an incident proton energy around 500 MeV, a minimum near 1 GeV and a gradual increase above 1.5 GeV. Graphite is found to be a good target material if the transmitted proton beam is to be used for other purposes, but in a stand alone source, nickel would also be a good choice.

ACKNOWLEDGEMENTS

The support for this work provided by the European Commission under the 7th Framework Programme through the Research Infrastructures action of the Capacities Program, NMI3-II Grant Number 283883, is gratefully acknowledged.

[1] S. F. J. Cox, J. Phys. C: Solid State Phys. 20 3187 (1987)
[2] A. Schenck, “Muon Spin Rotation Spectroscopy”, Adam Hilger, Bristol, 1985
[3] A. Yaouanc, P. Dalmas de Réotier, “Muon Spin Rotation, Relaxation and Resonance”, Oxford University Press, 2011.
[4] R. Heffner and K. Nagamine, “Special issue on μSR: muon spin rotation, relaxation or resonance”, J.Phys.: Condens. Matter, 16, No.40, 2004.
[5] S. L. Lee, S. H. Kilcoyne and R. Cywinski, “Muon Science (Muons in Physics, Chemistry and Materials), Institute of Physics Publishing, Bristol, Philadelphia, 1999.
[6] S. J. Blundell, “Spin-polarised muons in condensed matter physics”, Contemporary Physics 40, 175–192, 1999.
[7] E. Karlsson, “Solid state phenomena, as seen by muons, protons, and excited nuclei”, (Clarendon, Oxford 1995)
[8] J. Sonier, J. Brewer, R. Kiefl, “SR studies of vortex state in type-II superconductors”, Rev. Mod. Phys., 72, 769 (2000)
[9] P. Dalmas de Rotier and A. Yaouanc, “Muon spin rotation and relaxation in magnetic materials”, J. Phys. Condens. Matter 9 9113-9166 (1997)
[10] A. Schenck and F. N. Gygax, “Magnetic materials studied by muon spin rotation spectroscopy”, In: Handbook

of Magnetic Materials, edited by K.H.J. Buschow, Vol. 9 (Elsevier, Amsterdam 1995) 57–302
[11] A. Amato, "Heavy-fermion systems studied by SR techniques", Rev. Mod. Phys., 69, 1119 (1997)
[12] V. K. Anand *et al.*, "Ferromagnetic cluster spin-glass behaviour in PrRhSn3", Phys. Rev. B 85 (1), 014418, 2012.
[13] B. D. Patterson, "Muonium states in semiconductors", Rev. Mod. Phys. 60 69–159 (1988)
[14] V. Storchak, N. Prokovev, "Quantum diffusion of muons and muonium atoms in solids", Rev. Mod. Phys., 70, 929 (1998)
[15] E. Roduner, "The positive muon as a probe in free radical chemistry", Lecture Notes in Chemistry No. 49 (Springer Verlag, Berlin 1988)
[16] "Towards a Next Generation European Muon Source", NMI3/CONFORM Workshop, Cockcroft Institute, Daresbury, 2008.
[17] F. Foroughi *et al.* "Upgrading the PSI Muon Facility", Kluwer Academic Publishers, Hyperfine Interactions 138, 483–488, 2001.
[18] J. L. Beveridge *et al.* "Muon Facilities at TRIUMF", Hyperfine Interactions 32, Issue 1-4, 907–912, 1986.
[19] G. H. Eaton *et al.*, "The Muon Beamline at ISIS", Technical Report, Rutherford Appleton Laboratory, 1994.
[20] Y. Miyake *et al.* "J-PARC Muon Science Facility with use of 3 GeV Proton Beam", Nuclear Physics B (Proc. Suppl.) 149, 393–395, 2005.
[21] R. Cywinski, Phys.World 19, 13 (2006).
[22] GEANT4 — version 4.9.3.p02, CERN [http://geant4.cern.ch].
[23] A. Ribon *et al.*, Report No. CERN-LCGAPP, 2010.
[24] G. Folger *et al.*, Eur. Phys. J. A 21, 407, 2004.
[25] A. Heikkinen *et al.*, "Implementation of INCL4 cascade and ABLA evaporation codes in Geant4", Journal of Physics: Conference Series 119, 032024, 2008.
[26] D. R. F. Cochran *et al.*, Phys. Rev. D 6, 3085 (1972).
[27] Adriana Bungau *et al.*, "Simulations of Surface Muon Production in Graphite Targets", Phys. Rev. ST Accel. Beams 16, 014701 (2013).
[28] Michael Kelsey, SLAC, private communication.
[29] Adriana Bungau *et al.*, "Target optimization studies for surface muon production",Phys. Rev. ST Accel. Beams 17, 034701 (2014)
[30] G. H. Eaton, M. A. Clarke-Gayther, C. A. Scott, C. N. Uden and W. G. Williams, Nuclear Instruments and Methods A 342, 319 (1994).
[31] T. Matsuzaki, K. Ishida, K. Nagamine, I. Watanabe, G. H. Eaton and W. G. Willams, Nuclear Instruments and Methods A 465 365–383 (2001)